H$_2$-rich fluids from serpentinization: Geochemical and biotic implications

N. H. Sleep*†, A. Meibom‡, Th. Fridriksson†‡§, R. G. Coleman‡, and D. K. Bird‡

Departments of *Geophysics and ‡Geological and Environmental Sciences, Stanford University, Stanford, CA 94305

Metamorphic hydration and oxidation of ultramafic rocks produces serpentinites, composed of serpentine group minerals and varying amounts of brucite, magnetite, and/or FeNi alloys. These minerals buffer metamorphic fluids to extremely reducing conditions that are capable of producing hydrogen gas. Awaruite, FeNi$_3$, forms early in this process when the serpentinite minerals are Fe-rich. Olivine with the current mantle Fe/Mg ratio was oxidized during serpentinization after the Moon-forming impact. This process formed some of the ferric iron in the Earth's mantle. For the rest of Earth's history, serpentinites covered only a small fraction of the Earth's surface but were an important prebiotic and biotic environment. Extant methanogens react H$_2$ with CO$_2$ to form methane. This is a likely habitable environment on large silicate planets. The catalytic properties of FeNi$_3$ allow complex organic compounds to form within serpentinite and, when mixed with atmospherically produced complex organic matter and waters that circulated through basalts, constitutes an attractive prebiotic substrate. Conversely, inorganic catalysis of methane by FeNi$_3$ competes with nascent and extant life.

Ultramafic rocks, composed mainly of olivine and pyroxene (Mg and Fe^{2+} silicates), are a common feature in the lithospheres of early terrestrial planets. On early Earth these rocks formed by eruption as near total melts from the mantle, by solidification of cumulates from partial crystallization of mafic melts at shallow depths, and by exhumation from the mantle through impacts and tectonics. Tectonic exposure and cumulate formation of ultramafic rocks continue on modern Earth. The most common exposure today is along the axis of slow and very slow spreading ridges where the mantle is too cool to form significant basalt; ≈10% of oceanic crust forms at such ridges (1).

Here, we consider thermodynamic constraints on the formation of H$_2$-rich fluids by reaction of H$_2$O with ultramafic rocks at moderate temperatures and pressures. At temperatures <300°C and low concentrations of aqueous silica, these rocks react with H$_2$O to form hydrous Mg and Fe^{2+} silicates and hydroxides (2, 3). The fluid oxidizes some of the Fe^{2+} to magnetite liberating gaseous and aqueous H$_2$ to the environment, a process that can be observed today where hydrogen seeps occur on land, sometimes producing natural flames (4). Geochemists report hydrogen-bearing gases trapped in spring waters issuing from serpentinizing peridotites and ancient serpentinites undergoing modern weathering from Oman (5, 6), the Zambales ophiolite in the Philippines (4–8), Kansas oil wells (9, 10), the Sakalin and Koryak Plateau in Russia (11, 12), and Milford Sound in New Zealand (13). More recently, marine geologists discovered low-temperature fluids from vents rich in methane and hydrogen in midocean ridge systems (3, 14). The Lost City vent field along the mid-Atlantic ridge system supports microbial colonies with anaerobic thermophiles (3). Robert Rye (personal communication) has found similar microbial colonies within highly alkaline springs at the Cedars ultramafic complex in California, within the Franciscan trench melange (15).

Buffering of solutions by serpentinite mineral assemblages and production of H$_2$, considered in this study, are of interest to early biotic, and perhaps prebiotic, evolution on the Earth and other rocky planets. In addition, we suggest a global geochemical implication of H$_2$ production in the formation of ferric oxide in the Earth's mantle.

Biological Motivations

An important class of habitable environments supported by H$_2$ involves mixing of serpentinite-derived water with CO$_2$-rich water. The CO$_2$ reacts with H$_2$ to form methane by the reaction

$$4H_2 + CO_2 \rightarrow CH_4 + 2H_2O. \qquad [1]$$
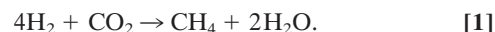
This reaction occurs abiotically in hydrothermal systems in serpentine (3, 16) and lower-temperature environments beneath oceans (17) and continents (18). Over geological time, metamorphism of carbonates and the degassing of lavas continually recharge ocean and atmosphere with CO$_2$.

Reaction **1** supports extant biota and abiotic processes. Methanogens in rocks can thrive at H$_2$ concentrations of ≈13 nM (19, 20), orders of magnitude below the concentration in equilibrium with serpentinite presented below. Magnetite and awaruite (FeNi$_3$, a common trace mineral in serpentinite) both catalyze methane production in the laboratory at hydrothermal conditions (21, 22). Complex organic matter forms abiotically from this process both in the laboratory and nature (3, 16, 18, 21, 22).

The formation of abiotic methane and more complex organic compounds is a boon to certain modern microbes that react them with photosynthetically generated oxygen (16, 20). This niche did not exist before life. Rather, abiotic methanogenesis was a mixed blessing to nascent life forms. Abiotic formation of methane competes with life by removing the energy source in reaction **1**. This is particularly true if awaruite or magnetite efficiently catalyzes the reaction (22). The reaction (along with the formation of MgCO$_3$) is also likely to occur when CO$_2$-rich water penetrates hot serpentine. This competition is evident in modern subsurface environments with a slow supply of the limiting reactant (either CO$_2$ or H$_2$) (18). Methanogens do exist there, but the abiotic consumption of their food reduces their productivity. There is a finite productivity below which abiotic processes outcompete life. At present, this limit is poorly constrained, but it could be fairly high for inept prebiotic autocatalysis and early life forms.

We continue with the positive aspects of serpentinization for life. Once life originated, methanogenesis was a continual subsurface niche on the Earth. This niche likely exists on Mars and Europa (16). The use of Ni, a common element in serpentinites and a rare element in other rocks, in the key enzyme of methanogens points to the great antiquity of this process on Earth and the probable origin of methanogenesis within fluids that reacted with serpentinite (23, 24).

The H$_2$-rich waters formed by low-CO$_2$ hydrothermal fluids circulating through utramafic rocks generate a ''Darwin soup'' by mixing with other fluids and organic substrates. Mixing produced disequilibria and gathered the full repertoire of biological
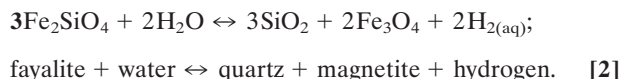
---

elements. First, the H_2 and the methane formed a very reduced atmosphere. Lightning is known to produce complex organic compounds in this situation (25). More transient reducing atmospheres from the oxidation of metallic Fe occurred after large asteroid impacts (26). In both cases, the presence of H_2 increases the yield of complex organic compounds (27). Similarly, complex organic compounds formed within the highly reducing subsurface environments in serpentinites (16).

Below, we provide examples of gathering of elements by flow through various serpentinite environments. Mixing may yield a solution enriched in several biologically important elements. For example, surface waters may contain amino acids formed from nitrogen, whereas ground waters in basalt may contain significant phosphorus. Finally, the strong catalytic properties of $FeNi_3$ grains in serpentinites make them a potential site for prebiotic chemistry. We are aware of no extant or fossil organisms that put these surfaces to a useful purpose or that use $FeNi_3$ within their cells. We feel that a diligent search is warranted.
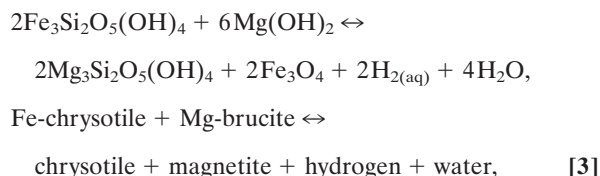
Rock–Water Reaction

To quantify our biological motivations, we compute concentrations of aqueous H_2 in fluids in equilibrium with serpentinites and the conditions where awaruite is stable. We use equilibrium thermodynamic relations to illustrate implications of a well known geologic process. We represent rocks as a mixture of minerals of limited compositional variation and the redox state in terms of the molality of aqueous H_2. In the case of ultramafic rocks, we consider the thermodynamic components H_2O, H_2, FeO, MgO, SiO_2, and NiO. We ignore sulfur and refer the reader to the work of Frost (28). Früh-Green *et al.* (3) discuss similar systems with significant carbon.

The mineralogy of ultramafic rocks is mostly olivine $[(Mg,Fe)_2SiO_4]$ and pyroxene [both orthopyroxenes (Mg,Fe)-SiO_3 and clinopyroxenes $Ca(Mg,Fe)Si_2O_6$], with atomic Mg/Fe ratios of $\approx 9{:}1$. Traditionally, the redox state of these geologic systems is controlled by the quartz-fayalite-magnetite (QFM) buffer, represented by equilibrium in the aqueous fluid for the reaction (29).

$$3Fe_2SiO_4 + 2H_2O \leftrightarrow 3SiO_2 + 2Fe_3O_4 + 2H_{2(aq)};$$

fayalite + water $\leftrightarrow$ quartz + magnetite + hydrogen.　　**[2]**

This buffer is relevant to redox conditions of ultramafic rocks under igneous conditions and the more silicic mafic rocks (30) even to temperatures of hydrothermal processes (31). Redox conditions defined by reaction **2** are inappropriate at temperatures $< \approx 300°C$ for ultramafic rocks, as the stable phases are serpentine $[(Mg,Fe)_3Si_2O_5(OH)_4]$, brucite $[(Mg,Fe)(OH)_2]$, and magnetite, where the activity of aqueous silica is far below that required to form quartz. Such hydrated metamorphic ultramafic rocks are called serpentinites (32).

During serpentinization of ultramafic rocks Mg and Fe^{2+} partition between serpentine and brucite so that the chemical potentials of MgO and FeO are the same in both phases (33, 34). We represent appropriate redox reaction for serpentinite by

$$2Fe_3Si_2O_5(OH)_4 + 6Mg(OH)_2 \leftrightarrow$$

$$2Mg_3Si_2O_5(OH)_4 + 2Fe_3O_4 + 2H_{2(aq)} + 4H_2O,$$

Fe-chrysotile + Mg-brucite $\leftrightarrow$

　　chrysotile + magnetite + hydrogen + water,　　**[3]**

where the stoichiometry corresponding to the Fe-chrysotile $[Fe_3Si_2O_5(OH)_4]$, chrysotile $[Mg_3Si_2O_5(OH)_4]$ and Mg-brucite $[Mg(OH)_2]$, and Fe-brucite $[Fe(OH)_2]$ denotes components of Mg-Fe^{2+} substitution in solid solution minerals of serpentine and

brucite, respectively. We base our thermodynamic evaluation of Fe^{2+} substitution in serpentine and brucite on the mineral compositions of geologic serpentinites (see *Appendix*). This analysis demonstrates the importance of modest Fe^{2+} substitution in these minerals on H_2 generation in planetary crusts.

Reaction **3** applies when there is enough Mg plus Fe(II) to form brucite; that is, $(Mg+Fe(II)) >1.5$ Si, as occurs in dunites [nearly monomineralic olivine with $(Mg+Fe(II)){:}Si = 2$] and some harzburgites (rocks with olivine and minor orthopyroxene). These rock types occurred on the ancient Earth (35). With a lower ratio $Mg+Fe(II)/Si$ than 1.5, the assemblage serpentine plus talc is more oxidized. We consider serpentine plus brucite as we are interested in the more reduced assemblage that equilibrates with a higher concentration of H_2. We recognize that the assemblage serpentine-brucite-magnetite (SBM) does form directly from olivine, and we restrict our analysis to equilibrium conditions near open fractures.
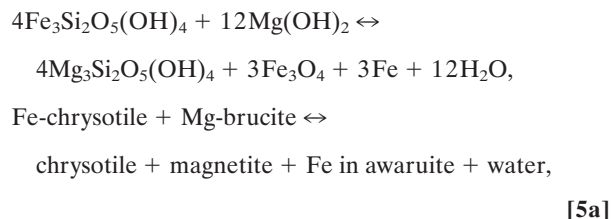
Metallic iron was present on the early Earth during accretion, just after the Moon-forming impact, and locally after major asteroid impacts. Awaruite, a Ni-rich alloy with compositions close to that of the ordered mineral Ni_3Fe, occurs within modern serpentinites (35, 36). The formation of awaruite in the presence of magnetite is of interest here because H_2 is produced during formation of magnetite from ferrous iron. We represent an additional set of redox reactions involving metallic Ni-Fe alloys as
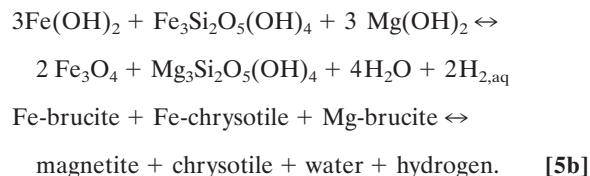
$$FeO + H_2 \leftrightarrow Fe + H_2O,　　\textbf{[4a]}$$

and

$$NiO + H_2 \leftrightarrow Ni + H_2O,　　\textbf{[4b]}$$

where Fe and Ni oxides denote thermodynamic components in SBM (reaction **3**), and Fe and Ni denote components in Ni-Fe alloy awaruite. Reaction **4a** allows us to represent equilibria between SBM (reaction **3**) and awaruite in terms of the activity of Fe in awaruite as:

$$4Fe_3Si_2O_5(OH)_4 + 12Mg(OH)_2 \leftrightarrow$$

$$4Mg_3Si_2O_5(OH)_4 + 3Fe_3O_4 + 3Fe + 12H_2O,$$

Fe-chrysotile + Mg-brucite $\leftrightarrow$

　　chrysotile + magnetite + Fe in awaruite + water,

[5a]

and

$$3Fe(OH)_2 + Fe_3Si_2O_5(OH)_4 + 3\ Mg(OH)_2 \leftrightarrow$$

$$2\ Fe_3O_4 + Mg_3Si_2O_5(OH)_4 + 4H_2O + 2H_{2,aq}$$

Fe-brucite + Fe-chrysotile + Mg-brucite $\leftrightarrow$

　　magnetite + chrysotile + water + hydrogen.　　**[5b]**

These reactions provide compositional constraints among serpentine and brucite in equilibrium with magnetite as a function of the activity of Fe in awaruite and the molality of H_2 (see *Appendix*).

Phase Equilibria

We compute phase equilibria by using thermodynamic data, standard state conventions, and solid solution approximations defined in *Appendix*. Our intent is to illustrate basic features of aqueous H_2 concentrations and fluid saturation with H_2 consistent with the common serpentinite mineral assemblages: (Mg-Fe)-chrysotile, (Mg-Fe)-brucite, and magnetite, for reactions in

EVOLUTION

GEOLOGY
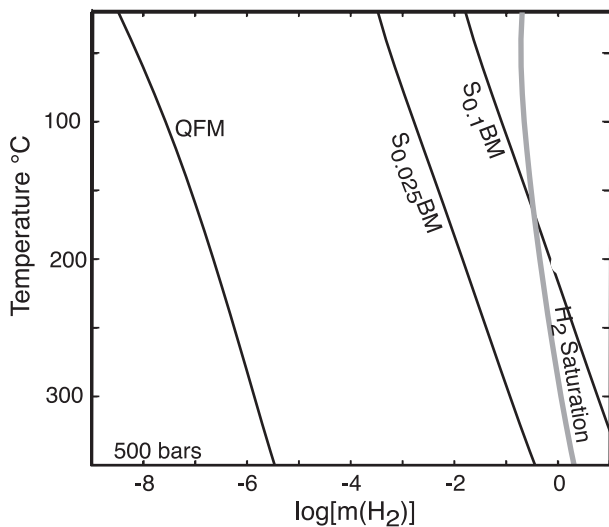
Fig. 1. Molality of $H_{2(aq)}$ for SBM buffer (reaction **3**) as a function of temperature at 500 bars total fluid pressure. Isopleth $S_{0.1}BM$ represents high-Fe serpentinite, with $X_{Fe} = 0.1$ in crysotile and $X_{Fe} = 0.07$ in brucite, and $S_{0.025}BM$ represents low-Fe serpentinite, with $X_{Fe} = 0.025$ in crysotile and 0.0175 in brucite. QFM buffer and hydrogen solubility bars are shown.

Fig. 2. Phase diagram as in Fig. 1 showing isopleths of SBM buffer equilibria for serpentinites with X_{Fe} in crysotile ranging from 0.1 to 0.025. H_2 partial pressure contours are thick gray lines.

open pore space where water can potentially ascend toward the surface of biological interest. We assume that abundant solid phases control the equilibrium of locally small amounts of fluid, composed mostly of H_2O. At temperatures >200°C, olivine and orthopyroxene hydrate to serpentine and brucite at laboratory time scales (37, 38). In rocks, the serpentine polymorph chrysotile grows within pore space, whereas the more common polymorph lizardite develops in the rock matrix (39), where relict olivine is commonly in contact with lizardite.

At Earth surface temperatures, olivine and orthopyroxene rapidly dissolve in ground waters, making the water supersaturated in serpentine and brucite that precipitate slowly (40). We cannot simply apply reaction **3** because kinetically controlled supersaturated reactants occur on both sides. It has not escaped us that disequilibrium between dissolved Fe(II), water, and the products magnetite and H_2 is a potential biotic reaction in this environment.

We present diagrams that help constrain mass balance of a biological or an industrial process based on aqueous H_2 in serpentinite. The concentration of H_2 per mass of fluid stays constant as a fluid-dominated region heats or cools, unless the fluid becomes saturated with respect to H_2 gas. This lets us represent a water-dominated part of fluid circulation, like a vein. We assume a fluid pressure of 500 bars, which is appropriate for high-level crustal rocks during the early Earth when much of its water had not yet entered the mantle and was either in the ocean or the atmosphere, and for modern reactions occurring ≈2 km deep in modern oceanic crust near ridge axes. The solid-phase equilibria and the computed partial pressure of hydrogen are not sensitive to pressure at temperatures below the critical point of water, ≈374°C and 220 bars.

Equilibria for the buffer reactions QFM (reaction **2**) and SBM (reaction **3**) equilibria are shown in Fig. 1 as a function of temperature and the molality of aqueous H_2. The isopleth labeled $S_{0.1}BM$ denotes equilibrium for reaction **3**, where the mole fraction $X_{Fe} \equiv Fe/(Mg+Fe)$ of Fe(II) in serpentine is 0.1 and X_{Fe} in the brucite is in equilibrium with the serpentine (see *Appendix*). The $S_{0.1}BM$ isopleth represents a "high-Fe(II)" system. For comparison, the isopleth-labeled $S_{0.025}BM$ represents equilibrium with "low-Fe(II)" substitution in serpentine and
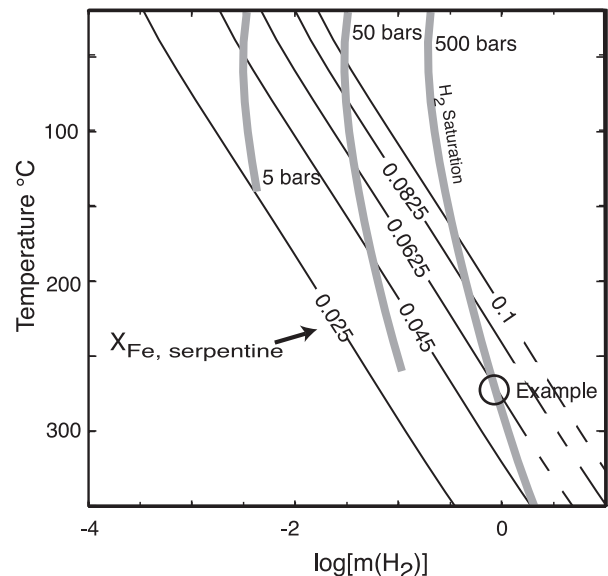
brucite. Note the differences of aqueous hydrogen concentrations required by the mineral buffers QFM and SBM and the sensitivity of $H_2(aq)$ concentrations of SBM equilibria to Fe(II) substitution. The curve labeled H_2 Saturation in Fig. 1 denotes saturation of the fluid with $H_{2(gas)}$ at 500 bars total fluid pressure (see *Appendix*); mineral reactions to the right of this saturation curve are metastable. If a more reduced phase is initially present (for example, metallic Fe), it is oxidized, producing hydrogen gas. Gas bubbles may build up in the fluid because the equilibrium does not depend on the amount of bubbles present. Reactions to the left of the solubility curve cannot saturate the fluid with $H_{2(gas)}$ at a total fluid pressure of 500 bars. Finally, note the curve $S_{0.1}BM$ in Fig. 1 represents the initial stage of oxidation in the early Earth and that of modern alpine peridotite. The atomic fraction X_{Fe} is 0.1 in serpentine and ≈0.18 in brucite ($S_{0.1}B_{0.18}M$), in total X_{Fe}, being approximately the same as in primary ultramafic rocks, since the mode of serpentine is much larger than that of brucite.

$S_{0.1}BM$ is an effective buffer in serpentinites. The addition of hydrogen to a previously closed system equilibrium will result in reduction of magnetite, which consumes some of the added hydrogen and some of the magnetite. The new equilibrium has increased hydrogen pressure and increased X_{Fe} in serpentine and brucite.

Fluids buffered by the assemblage $S_{0.1}BM$ (Fig. 1) are supersaturated with respect to $H_{2(gas)}$ at temperatures more than ≈160°C. The buffer assemblage $S_{0.025}BM$ (Fig. 1) represents an extensively oxidized serpentinite, where most of the Fe is in magnetite and $X_{Fe} = 0.025$ in serpentine and $X_{Fe} = ≈0.05$ in brucite ($S_{0.025}B_{0.05}M$). Fluids in equilibrium with serpentine and brucite of these compositions are undersaturated with respect to $H_{2(gas)}$ at all temperatures shown in Fig. 1. The oxidation reaction still may proceed if the H_2 concentration is undersaturated with $H_{2(gas)}$. We expect this situation when fluid vigorously circulates through the rock, removing dissolved hydrogen. The hydrogen-enriched fluid then vents to the surface and is replaced at depth with hydrogen-poor fluid from the ocean.

Fig. 2 illustrates the SBM buffer equilibrium as a function of temperature and $H_{2(aq)}$ concentrations for serpentine compositions ranging from X_{Fe} 0.025 to 0.1. The curve labeled 500 bars denotes fluid saturation with respect to $H_{2(gas)}$ and the curves

Sleep *et al.*
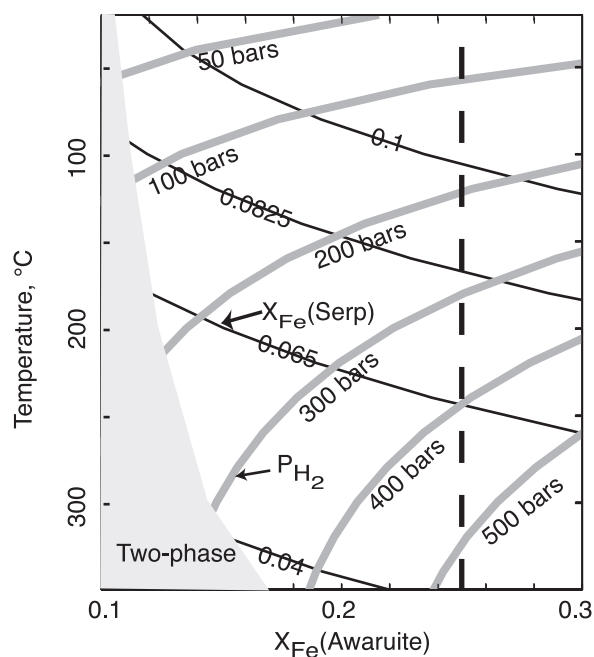
Fig. 3. Hydrogen partial pressures and X_{Fe} in serpentine in equilibrium with brucite, magnetite, and awaruite as a function of X_{Fe} in awaruite and temperature. The two-phase region (awaruite plus Ni solid solution) is shaded.

Fig. 4. Examples of two paths of fluid composition on phase diagram as in Fig. 2. The path A–F represents venting of fluid in a deep system on land that is initially in equilibrium with serpentinite at point A. The second path (R–S–A–B–C–R) represents circulation beneath a massive H_2 atmosphere on the early Earth.

labeled 5 and 50 bars represent isopleths of $H_{2(gas)}$ partial pressures. Note in Fig. 2 that equilibrium of SBM with $H_{2(gas)}$ saturated fluid requires an increase in the Fe(II) content of serpentine and brucite with decreasing temperature. Similar features are apparent for the cooling of fluids at constant partial pressures of $H_{2(gas)}$. As an example, consider reaction at 260°C of H_2-saturated fluid and an initial Fe-rich serpentinite (with X_{Fe} serpentine of 0.01), reaction will proceed until $H_{2(gas)}$, magnetite, serpentine, brucite, and water are in equilibrium for X_{Fe} in serpentine of 0.0625 and X_{Fe} in brucite is ≈ 0.12 ($S_{0.065}B_{0.12}M$). The quick yield of hydrogen is that needed to oxidize the rock to this composition. Any further oxidation would lower Fe/Mg in serpentine and brucite, leaving the fluid undersaturated with respect to hydrogen. Conversely, X_{Fe} in serpentine forms in equilibrium only on the left side of the $H_{2(gas)}$ saturation curve. For example, at 50-bar partial pressure of $H_{2(gas)}$ and 120°C would have X_{Fe} in serpentine < 0.0625.

The stability field of the Ni-Fe alloy awaruite in the presence of serpentine, brucite, and magnetite is shown in Fig. 3, which illustrates the two-phase field of Ni-rich solid solutions plus awarurite (shaded area), and the region of awaruite stability (see *Appendix*). Also shown are isopleths (solid curves) of X_{Fe} in serpentine for the assemblage serpentine, brucite, magnetite, and awaruite as represented by equilibrium for reaction **5a**, and isopleths (shaded curves) of partial pressures of $H_{2(gas)}$ consistent with reactions **5b** and **S3** in *Appendix*. The curve labeled 500 bars denotes $H_{2(gas)}$ saturation in the fluid, and the vertical dashed line denotes the composition of stoichiometric awaruite ($FeNi_3$). Fig. 3 is compatible with previous thermodynamic relations and field observations (3, 28). That is, late magnetite-bearing assemblages replace earlier awaruite-bearing ones as the rock becomes increasing oxidized (3). Note that there is a minimum X_{Fe} in serpentine for awaruite to be stable, which decreases with increasing temperature, which is a weak function of X_{Fe} in awaruite. The partial pressure of H_2 needed to form awaruite increases with temperature. For example, at 200°C, awaruite of composition $FeNi_3$ cannot form unless the H_2 partial pressure is more than ≈ 320 bars, which would preclude awaruite formation in
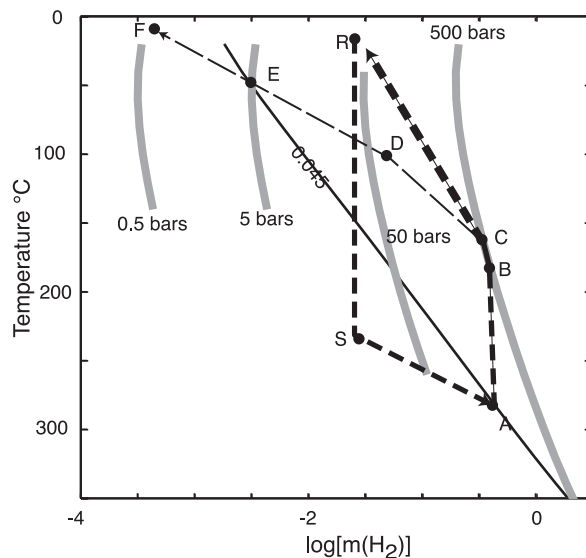
a shallow land system. Even at low temperature, partial pressures in excess of 50 bars H_2 is needed to form awaruite.

Ascent and Venting of Hydrogen-Rich Water

Observations of hydrothermal vents at oceanic spreading centers and off-axis locations (17), together with mineralogic and isotopic measurements of fossil magma-hydrothermal and regional metamorphic terrains, demonstrate that aqueous fluids locally flow in large quantities in crustal rocks (41–43). Metasomatic reaction zones around veins in these rocks indicate that fluids rapidly react with their lithologic environment.

Fig. 4 illustrates hypothetical paths of fluid-dominated phase relations during cooling within an idealized serpentinite. Fluid in equilibrium with the local composition of serpentine, brucite, and magnetite is represented by pressure-temperature point A in Fig. 4. The fluid then cools to point B where it becomes saturated with hydrogen. It continues to cool to point C, losing hydrogen to bubbles. Finally, it ascends upward to lower pressures and temperatures, losing more hydrogen into bubbles along the path D–E–F. It vents on land at point F. Essentially all of the hydrogen originally in solution at point A escapes as bubbles. Between points A and E, the fluid is more reducing than the serpentine from which it formed. The fluid may locally react with the rock, consuming magnetite as represented by reaction **3**. Boiling may produce locally hydrogen-rich fluids. In general, a boiled fluid once quenched is likely to be saturated with hydrogen. This process is relevant to producing hydrogen seeps on land where the total pressure is low.

Moon-Forming Impact and Ferric Iron in the Earth's Mantle

The Earth's Moon formed when a Mars-sized object collided with the Venus-sized Proto-Earth. As summarized by Sleep *et al.* (44), the impact left the Earth surrounded by a rock-vapor atmosphere, which condensed in a few thousand years. The Earth's water and CO_2 formed a dense atmosphere heated from below. Internal heating became an insignificant effect on climate after ≈ 2 million years. By that time, liquid oceans condensed beneath a dense CO_2 atmosphere, and the surface temperature was ≈ 200°C. The Earth's gravity was able to hold CO_2, water,

and significant H_2. In contrast, the Moon did not retain these gases and lacks potentially habitable ground water.

Thereafter, the capacity of the Earth's surface rocks to hold CO_2 in carbonates controlled the CO_2 pressure and hence (along with methane) climate (44–46). Rocks of the lithocap of this magma ocean were, however, insufficient to contain the available CO_2. Rather, the Earth's interior sequestered CO_2 when the surface layer foundered, a process analogous to modern subduction of carbonates in altered oceanic basalts. This storage required that the foundered crust did not immediately degas its CO_2. Instead much of the CO_2 mixed into the deep interior (47). This situation prevails now in that only a modest fraction of subducted CO_2 immediately returns to the surface at arc volcanoes.

Our concern here is the effect of the aftermath of the Moon-forming impact on oxidation state of the Earth's mantle. The Earth's mantle contains a significant amount of ferric iron that is out of equilibrium with metallic iron in accreting bodies, which formed the Earth's core (e.g., ref. 48). Ferric iron probably formed after the bulk of Earth's metallic iron was sequestered in the core, at least partially after the Moon-forming impact. In addition, a "veneer" component of platinum group elements exists in the Earth's mantle. This material formed along with the oxidation of metallic iron, much from the core of the impacting body. Water and preexisting ferric iron in the Proto-Earth's mantle are the probable oxidants.

Mass balance indicates that that these processes produced massive amounts of hydrogen gas (e.g., ref. 48). The ferric iron requires reduction of 4.5×10^{22} mol of water (60% of the mass of the current hydrosphere) to H_2. The platinum-group elements require 7.5×10^{22} mol of water (about the mass of the current hydrosphere). The hydrogen gas from each source (if all in the air at the same time) would have produced equivalent pressures of 20 and 30 bars, respectively for a total of 50 bars. That is, an equivalent pressure of 50 bars is a reasonable upper limit for the amount of H_2 in the aftermath of the Moon-forming impact.

The relative timing of the escape of atmospheric H_2 to space and the demise of CO_2 by forming carbonates is unknown. In addition, much of the hydrogen production (partially that from the oxidation of metallic iron) occurred at magmatic temperatures inside the Earth or when the Earth's surface was still too hot for liquid water to form. Our calculations are inapplicable for a massive CO_2 atmosphere as carbon species are not included. However, we can represent the behavior of a clement massive hydrogen atmosphere above the liquid-water ocean.

We consider the behavior of serpentine with the Fe^{+2}/Mg ratio of the present mantle, by using Fig. 2. If no redox reactions occur this rock forms serpentinite with X_{Fe} in serpentine of ≈0.1, which produces hydrogen at 160°C at all reasonable H_2 atmospheric partial pressures. At 20°C, this serpentinite is in equilibrium with 30 bars of H_2 and produces H_2 at lower H_2 pressures. Even in the extreme case of 50 bars of surface H_2, oxidation of serpentinite proceeds during hydrothermal circulation. For example, fluid saturated with 50 bars of H_2 descends from recharge point R (Fig. 4) into the subsurface as a closed system to point S. It then heats up and reaches equilibrium with moderately oxidized serpentinite at point A. The water then ascends back to the surface, forming bubbles along the way on the path B–C–R. More than 90% of the H_2 present at point A eventually forms bubbles and escapes to the surface.

Thus significant oxidation of the mantle could have occurred at hydrothermal conditions on the early Earth or on other bodies where ultramafic rocks covered the surface. Conversely, the process on Earth was inefficient enough that most of the mantle's iron is still ferrous, not 2/3 ferric, as in magnetite. Also, we still have an ocean. There is no obvious hydrothermal buffer that would yield the current mantle composition from a long-lived equilibrium process.

## Conclusions About the Later History of the Earth

Ultramafic rocks are uncommon on the surface of the modern Earth. This situation prevailed soon after the Moon-forming impact when the Earth's interior cooled to the point where the most common igneous rock was basalt, formed by partial melting of the mostly solid mantle. The dominant buffer since that time has been approximately QFM (reaction **2**). Although uncommon, serpentinized ultramafic rocks are important biotic environments on the modern Earth. They are also likely to have been a prebiotic environment on any silicate planet. These situations are likely to resemble the modern Earth, where both low- and high-temperature hydrothermal circulation occurs.

Figs. 2 and 3 suffice to delineate the environments where H_2 may be generated, and where the minerals magnetite and $FeNi_3$ may form. H_2 forms in molar to millimolar quantities at all temperatures even after much of the ferric iron in serpentine is oxidized. This finding is compatible with the observation of hydrogen in warm (40–70°C) oceanic hydrothermal vents (17), hot hydrothermal vents (16), 2-km deep waters within the Canadian Shield (18), and even natural flames above seeps on land (4). Magnetite is a stable phase in these environments. In contrast, $FeNi_3$ forms only at high X_{Fe} in serpentine, and hence high H_2 pressure. It is not expected to form at shallow depths or once the serpentinite is extensively oxidized. The presence of this mineral in surface samples and placers, however, indicates that it oxidizes quite slowly at modern surface temperatures.

Appendix: Thermodynamic Calculations

We compute the phase relations depicted in Figs. 1–4 for equilibrium of reactions **1**, **3**, and **5** by using equilibrium constants derived from SUPCRT92 (49). Standard state conventions are unit activity at any temperature and pressure for stoichiometric minerals and H_2O, unit activity of a hypothetical one molal solution at infinite dilution for aqueous species, and unit activity of pure gases at any temperature and one bar.

We assume unit activities of quartz, magnetite, and water and compute activities of other solid phases, assuming ideal site-mixing solid solutions. The activity of fayalite is equal to 0.0064, which corresponds to the mole fraction of fayalite in olivine of mantle composition (0.08). We considered several compositions of serpentine (Fe-Mg chrysotile) and Fe-Mg brucite; activities of mineral components chrysotile, Fe-chrysotile, Mg-brucite, and Fe-brucite (i.e., $a_{Fe\text{-}chrysotile} = X^3_{Fe,chrysotile}$ and $a_{Fe\text{-}brucite} = X_{Fe,brucite}$, and vice versa for the Mg-endmembers) are computed consistent with the exchange reaction

$$3\ Fe(OH)_2 + Mg_3Si_2O_5(OH)_4 \leftrightarrow$$
$$Fe_3SiO_5(OH)_4 + 3\ Mg(OH)_2 \qquad \textbf{[S1]}$$
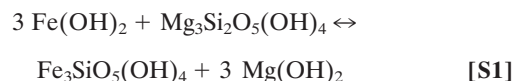
using a distribution coefficient of $K_d = 0.5$ reported by Evans and Trommsdorff (50), which is based on coexisting compositions of lizardite and brucite from serpentinites reported in the literature. The ratio of the mole fraction of Fe(II) in brucite to serpentine solid solutions is ≈2, which we assume to be independent of temperature and pressure at <300°C and 500 bars.

We compute the activity of Fe in $FeNi_3$ (awaruite) considering the stability of completely disordered $FeNi_3$ phase that corresponds to Fe metal with the activity of Fe equal to 0.25. We then compute the activity of ordered awaruite by noting that the entropy difference between the two ordering states is equal to the configurational entropy S_{con} (S_{con} is zero in the ordered phase and equal to 1.12 cal·mol^{-1}·K^{-1} per atom in the formula unit for the disordered phase) and that the order/disorder transition temperature is equal to 500°C (28). Finally, the activity coefficient of $H_{2,aq}$ as a function of temperature was calculated by using EQ3 (51) and the b-dot extended Debye-Huckel equation for a model sea water solution.

Thermodynamic data for H_2O, $H_{2(aq)}$, $H_{2(g)}$, and minerals (except metallic iron and Fe-brucite) are from the slop98.dat database (ref. 49 and http://geopig.asu.edu/supcrt92_data/slop98.dat). As a first-order approximation we use the thermodynamic data for greenalite reported in the slop98 database for Fe-chrysotile. We used thermodynamic data for metallic iron from Robie and Hemingway (52). Gibbs energy of formation and enthalpy of formation for Fe-brucite from Wagman *et al.* (53), which is consistent with Weast (54). Heat capacity of Fe-brucite is estimated by assuming zero heat capacity for the reaction

$$2\,Fe(OH)_2 + Mg_2SiO_4 \leftrightarrow 2\,Mg(OH)_2 + Fe_2SiO_4 \quad [S2]$$

using heat capacity data from Helgeson *et al.* (55). Molar volume of Fe-brucite is based on density measurements of $Fe(OH)_2$ by Kozlov and Levshov (56).

Solubility curves of $H_{2,g}$ in water in Figs. 1–4 denote equilibrium for

$$H_{2,g} \leftrightarrow H_{2,aq} \quad [S3]$$

as a function of temperature at 30, 500 bars, etc. by using SUPCRT92 (49). We assume that H_2 behaves as an ideal gas under the pressure and temperature conditions considered. H_2 solubility curves represent the solubility of a pure H_2 gas.

1. Dick, H. J. B., Lin, J. & Schouten, H. (2003) *Nature* **426,** 405–412.
2. Hemley, J. J., Montoya, J. W., Shaw, D. R. & Luce, R. W. (1977) *Am. J. Sci.* **277,** 353–383.
3. Früh-Green, G. L., Connolly, J. A. D., Plas, A., Kelley, D. S. & Grobéty, B. (2004) *AGU Mongr.*, in press.
4. Abrajano, Y. A., Sturchio, N. C., Bohlke, J. K., Lyon, G. L., Pordea, R. J. & Stevens, C. M. (1988) *Chem. Geol.* **71,** 211–222.
5. Barnes, I., O'Neil, J. R. & Trescases, J. J. (1978) *Geochim. Cosmochim. Acta* **42,** 144–145.
6. Neal, C. & Stanger, G. (1983) *Earth Planetary Sci. Lett.* **66,** 315–320.
7. Abrajano, T. A., Sturchio, N. C., Kennedy, B. M., Lyon, G. L., Muehlenbachs, K. & Bohlke, J. K. (1990) *Appl. Geochem.* **5,** 625–630.
8. Sturchio, N. C., Abrajano, T. A., Murdwchick, J. & Muelenbachs, K. (1989) *Tectonophysics* **168,** 101–107.
9. Coveney, R. M. (1971) *Econ. Geol.* **66,** 1265–1266.
10. Coveney, R. M., Jr., Goebel, E. D., Zeller, E. J., Dreschhoff, G. A. M. & Angino, E. E. (1987) *Am. Assoc. Petroleum Geol. Bull.* **71,** 39–48.
11. Yurkova, R. M., Slonimskyaya, M. V., Dainiyak, B. A. & Drits, V. A. (1982) *Dokl. Akad. Nauk SSSR* **263,** 420–425.
12. Velinski, V. V. (1978) *Geol. Geofiz.* **3,** 52–62.
13. Wood, B. L. (1970) *New Zealand J. Geol. Geophys.* **15,** 88–128.
14. Kelley, D. S. & Früh-Green, G. L. (1999) *J. Geophys. Res.* **104,** 10439–10460.
15. Barnes, I., LaMarche, V. C. & Himmelberg, G. (1967) *Science* **156,** 830–832.
16. Holm, N. G. & Charlou, J. T. L. (2001) *Earth Planet. Sci. Lett.* **191,** 1–8.
17. Kelley, D. S., Karson, J. A., Blackman, D. K., Früh-Green, G. L., Butterfield, D. A., Lilley, M. D., Olson, E. J., Schrenk, M. O., Roe, K. K., Lebon, G. T., *et al.* (2001) *Nature* **412,** 145–149.
18. Sherwood Lollar, B., Westgate, T. D., Ward, J. A., Slater, G. F. & Lacrampe-Couloume, G. (2002) *Nature* **416,** 522–524.
19. Kral, T. A., Brink, K. M., Miller, S. L. & McCay, C. P. (1998) *Origins Life Evol. Biosphere* **28,** 311–319.
20. Chapelle, F. H., O'Neill, K., Bradley, P. M., Methé, B. A., Ciufo, S. A., Knobel, L. L. & Lovley, D. R. (1997) *Nature* **1202,** 312–315.
21. Berndt, M. E., Allen, D. E. & Seyfried, W. E., Jr. (1996) *Geology* **24,** 351–354.
22. Horita, J. & Berndt, M. E. (1999) *Sciences* **285,** 1055–1057.
23. Nisbet, E. G. & Fowler, C. M. R. (1982) in *Tectonic and Biological Segmentation of Mid-Ocean Ridges*, eds. MacLeod, C. J., Tyler, P. A. & Walker, C. L. (Geological Society, London), Spec. Pub. 188, pp. 239–251.
24. Fraústo da Silva, J. J. R. & Williams, R. J. P. (2001) *The Biological Chemistry of the Elements: The Inorganic Chemistry of Life* (Oxford Univ. Press, New York), 2nd Ed.
25. Miller, S. L. & Urey, H. (1959) *Science* **130,** 245–251.
26. Kasting, J. F. (1990) *Origin Life Evol. Biosphere* **20,** 199–231.
27. Miyakawa, S., Yamanashi, H., Kobayashi, K., Cleaves, H. J. & Miller, S. L. (2002) *Proc. Natl. Acad. Sci. USA* **99,** 14628–14631.
28. Frost, B. R. (1985) *J. Petrol.* **26,** 31–63.
29. Basaltic Volcanism Study Project (1981) *Basaltic Volcanism on the Terrestrial Planets* (Pergamon, New York).
30. Morse, S. A., Lindsley, D. H. & Williams, R. J. (1980) *Am. J. Sci.* **280,** 159–170.
31. Bird, D. K., Rogers, R. D. & Manning, C. E. (1986) *Meddelelser Grønland* **16,** 1–68.
32. Coleman, R. G. (1971) *Geol. Soc. Am. Bull.* **82,** 897–917.
33. Coleman, R. G. & Jove, C. (1993) in *The Vegetation of Ultramafic (Serpentine) Soils*, ed. Reeves, R. D. (Intercept, Andover, U.K.), pp. 1–17.
34. O'Hanley, D. S. (1996) *Serpentinites: Records of Tectonic and Petrological History* (Oxford Univ. Press, New York).
35. Eckstrand, O. R. (1975) *Econ. Geol.* **70,** 183–201.
36. Railton, G. L. & Watters, W. A. (1990) *New Zealand Geol. Survey Bull.* **104,** 1–89.
37. Martin, B. & Fyfe, W. S. (1970) *Chem. Geol.* **6,** 185–202.
38. Wegner, W. W. & Ernst, W. G. (1983) *Am. J. Sci.* **283,** 151–180.
39. Evans, B. W. (2004). *Int. Geol. Rev.* **46,** 479–506.
40. Nesbitt, H. W. & Bricker, O. P. (1978) *Geochim. Cosmochim. Acta* **42,** 403–409.
41. U. S. National Research Council, Commission on Geosciences, Environment, and Resources, Geophysics Study Committee (1990) *The Role of Fluids in Crustal Processes* (Natl. Acad. Press, Washington, DC).
42. Lasaga, A. C., Rye, D. M., Lüttge, A. & Bolton, E. W. (2001) *Geochim. Cosmochim. Acta* **65,** 1161–1185.
43. Ingebritsen, S. E. & Manning, C. E. (2002) *Proc. Natl. Acad. Sci. USA* **99,** 9113–9116.
44. Sleep, N. H., Zahnle, K. & Neuhoff, P. S. (2001) *Proc. Natl. Acad. Sci. USA* **98,** 3666–3672.
45. Sleep, N. H. & Zahnle, K. (2001) *J. Geophys. Res.* **106,** 1373–1399.
46. Pavlov, A. A., Kasting, J. F., Brown, L. L., Rages, K. A. & Freedman, R. (2000) *J. Geophys. Res.* **105,** 11981–11900.
47. Keppler, H., Wiedenbeck, M. & Shcheka, S. S. (2003) *Nature* **424,** 414–416.
48. Kuramoto, K. & Matsui, T. (1996) *J. Geophys. Res.* **101,** 14909–14932.
49. Johnson, J. W., Oelkers, E. H. & Helgeson, H. C. (1992) *Comput. Geosci.* **18,** 899–947.
50. Evans, B. W. & Trommsdorff, V. (1972) *Schweiz. Mineral. Petrogr. Mitte.* **52,** 251–256.
51. Wolery, T. J. (1991) EQ3NR, *A Computer Program for Geochemical Aqueous Speciation Solubility Calculations: Theoretical Manual, User's Guide, and Related Documentation* (Lawrence Livermore National Laboratory, Livermore, CA), Version 7.0.
52. Robie, R. A. & Hemingway, B. S. (1995) *Thermodynamic Properties of Minerals and Related Substances at 298.15 K and 1 Bar (105 Pascals) Pressure and at Higher Temperatures* (U.S. Geological Survey, Washington, DC), Bulletin B2131.
53. Wagman, D. D., Evans, W. H., Parker, V. B., Schumm, R. H., Halow, I., Bailey, S. M., Churney, K. L. & Nuttall, R. L. (1982) *J. Phys. Chem. Ref. Data* **11,** Suppl. 2, **2-1–2-392.**
54. Weast, R. C., ed. (1984) *CRC Handbook of Chemistry and Physics* (CRC, Boca Raton, FL).
55. Helgeson, H. C., Delany, J. M., Nesbitt, H. W. & Bird, D. K. (1978) *Am. J. Sci.* **278,** 1–229.
56. Kozlov, T. & Levshov, P. P. (1962) *Am. Mineral.* **47,** 1218–1218 (Russian translation).

EVOLUTION

GEOLOGY